THE JOURNAL OF PHYSICAL CHEMISTRY Letters

Letter

pubs.acs.org/JPCL

# Open Circuit Potential Build-Up in Perovskite Solar Cells from Dark Conditions to 1 Sun

Laxman Gouda, Ronen Gottesman, Adam Ginsburg, David A. Keller, Eynav Haltzi, Jiangang Hu, Shay Tirosh, Assaf Y. Anderson, and Arie Zaban*

Department of Chemistry, Center for Nanotechnology & Advanced Materials, Bar-Ilan University, Ramat Gan 52900, Israel

Pablo P. Boix*

Energy Research Institute @NTU, Nanyang Technological University, 50 Nanyang Drive, Research Techno Plaza, X-Frontier Block, Level 5, Singapore, 637553

Supporting Information

**ABSTRACT:** The high open-circuit potential ($V_{oc}$) achieved by perovskite solar cells (PSCs) is one of the keys to their success. The $V_{oc}$ analysis is essential to understand their working mechanisms. A large number of $CH_3NH_3PbI_{3-x}Cl_x$ PSCs were fabricated on single large-area substrates and their $V_{oc}$ dependencies on illumination intensity, $I_0$, were measured showing three distinctive regions. Similar results obtained in $Al_2O_3$ based PSCs relate the effect to the compact $TiO_2$ rather than the mesoporous oxide. We propose that two working mechanisms control the $V_{oc}$ in PSCs. The rise of $V_{oc}$ at low $I_0$ is determined by the employed semiconductor n-type contact ($TiO_2$ or MgO coated $TiO_2$). In contrast, at $I_0$ close to AM1.5G, the employed oxide does not affect the achieved voltage. Thus, a change of regime from an oxide-dominated $E_{Fn}$ (as in the dye sensitized solar cells) to an $E_{Fn}$, directly determined by the $CH_3NH_3PbI_{3-x}Cl_x$ absorber is suggested.

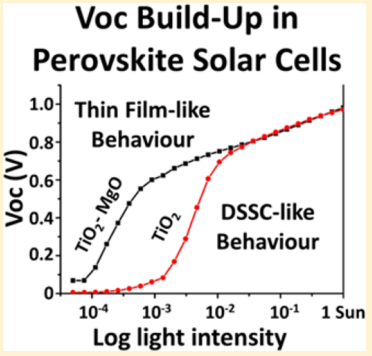


The first reports of hybrid halide perovskites methylammonium lead iodide $CH_3NH_3PbI_3$ and the mixed halide $CH_3NH_3PbI_{3-x}Cl_x$ solar cells (PSCs)[1,2] shook the field of solution-processed photovoltaics because of their unprecedented high performances. Three years later, with efficiencies above 20%,[3] perovskites devices are one of the most promising technologies, attracting the attention of both academic and industrial areas. These excellent semiconductors, with extraordinary suitable electrical,[4,5] optical,[6] and tailoring[7] characteristics have also been recently employed for LEDs, photodetectors, and transistors as well as for laser applications.[8−11]

Further development toward an applied technology requires a full understanding of the fundamental processes controlling the optoelectronic performance of perovskite devices. This knowledge is essential to answer still-open questions such as the origin of the hysteresis in current−voltage curves[12,13] and will help to elucidate the optimal device architecture. Since the early studies on PSCs, the use of electron conducting or nonconducting porous scaffolds (e.g., $TiO_2$ and $Al_2O_3$) has been a matter of discussion.[14] Particularly, the question still remains as to whether $TiO_2$ is maintaining its role as it does in the solid dye sensitized solar cells (DSSC)[15,16] in determining the $V_{oc}$ vs the hole transport material, or does it function simply as a contact, being that it is the perovskite that determines the potential. To answer that, further studies of the Voc and device energetics which focus on the contacts,[17,18] recombination,[19,20] and the role of the scaffold[21,22] are necessary.

In this work, we studied the $TiO_2$ interface with the perovskite absorber on the solar cell performance, with different thicknesses of $TiO_2$ blocking layer, focusing on the origin of the $V_{oc}$. The $TiO_2$/perovskite interface was studied by coating a thin MgO layer on the $TiO_2$ prior to the perovskite deposition, followed by measuring the $V_{oc}$ ($I_0$) behavior. The measurement of the $V_{oc}$ dependence on the illumination intensity under steady-state conditions is a basic characterization method that has been frequently used in the DSSC studies.[23,24] We measured the open-circuit potential in PSCs under a range of illumination intensities ($5 \times 10^{-5}$ sun < $I_0$ < 1 sun) which allowed us to observe three different $V_{oc}$ vs log $I_0$ regimes. From careful examination of the $V_{oc}$ vs log $I_0$ behavior, we propose that at very low light intensities the $V_{oc}$ is determined by the $TiO_2$ in a DSSC-like mechanism and ∼0.7 V from the maximum $V_{oc}$ (∼1 V at 1 sun) are contributed by the $TiO_2$. When $I_0$ approached 1 sun the metal oxide acted purely as a contact and ∼0.3 V of the $V_{oc}$ is contributed by the perovskite. In order to check our premise, we slightly changed the energetics of the $TiO_2$ by depositing an extremely thin layer of MgO on its surface. The change of energetics significantly altered the onset of $V_{oc}$ vs log $I_0$; however, the dual-mechanism at different light intensities remained the same.

**Received:** September 11, 2015
**Accepted:** November 9, 2015
**Published:** November 11, 2015




DOI: 10.1021/acs.jpclett.5b02014
J. Phys. Chem. Lett. 2015, 6, 4640−4645

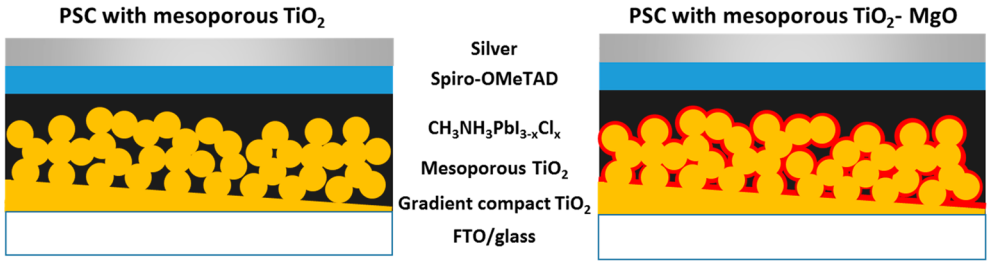


**Figure 1.** PSC with mesoscopic $TiO_2$ (left) and a PSC with mesoscopic $TiO_2$–MgO (right).

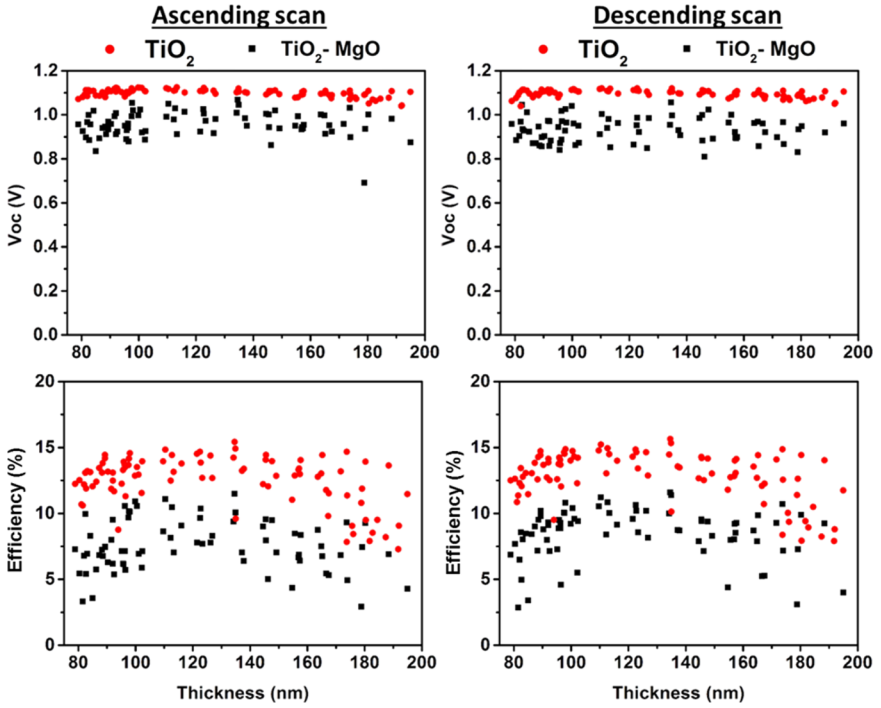


**Figure 2.** $V_{oc}$ and $P_{max}$ parameters from ascending and descending scans of the $TiO_2$ and $TiO_2$–MgO PSCs libraries vs thickness of the $TiO_2$ blocking layer.

Our approach leverages from the fabrication and measurements of a large number of solar cells on a single large-area substrate. This approach was developed in our laboratory and is also used for materials combinatorial studies[25,26] and all-oxide based photovoltaics research.[27] Following fabrication, the multiple cells are measured and analyzed via high throughput techniques, which provide accurate statistics on many properties of the solar cells. Typically, in one procedure we measure 121 $CH_3NH_3PbI_{3-x}Cl_x$ perovskite solar cells on a single large-area substrate, termed as a PSCs "library" (see Experimental Methods for full details). We have studied two types of libraries: (i) PSCs with mesoporous $TiO_2$ and (ii) PSCs with mesoporous $TiO_2$ and a thin layer (~2 nm) of MgO, which allowed identification of the role of the electron collector oxide. In both cases, the thickness of the gradient $TiO_2$ compact layer ranged from 80 to 195 nm (See Figure 1).

In order to elucidate the effect of the compact layer thickness on the photovoltaic performance, the current–voltage characteristics for each cell were measured under $I_0$ = AM1.5G in both ascending and descending voltage sweeps. The distribution of the photovoltaic parameters in Figure 2 displays an optimum compact $TiO_2$ thickness of ~135 nm for both $TiO_2$ and $TiO_2$–MgO libraries. The photovoltaic performance of the $TiO_2$ devices presents higher maximum power conversion efficiency of 15.1% with a general enhancement of all the photovoltaic parameters (Supporting Information (SI) Figure S1), whereas for the optimum thickness of the $TiO_2$–MgO devices the highest efficiency is 11.6%. At higher thicknesses, the $J_{sc}$ and FF decrease and spread their values (SI Figure S2), presumably due to a reduction of the charge collection and increase of the series resistance. PSCs with thinner compact layers showed a reduction in the fill factor, which is correlated to a small increase in the dark leakage current, as seen in SI Figure S3. As a result, the efficiency and the reproducibility of the parameters improved with the thickness of the compact layer.

More interestingly, when both the $TiO_2$ and $TiO_2$–MgO libraries were measured at steady state under different light intensities, the $V_{oc}$ vs log $I_0$ profiles showed very distinctive patterns.

In Figure 3a–c, three regions are evident for both libraries, although the $TiO_2$–MgO library had a $V_{oc}$ onset at lower $I_0$ values. PSCs with different compact layer thicknesses showed similar $V_{oc}(I_0)$ behaviors, as seen in Figure 3a, b. In Region I, at low $I_0$, the open circuit potential remains low with little increase ($V_{oc}$ < 200 mV). In Region II, at higher $I_0$, $V_{oc}$ increases abruptly (200 mV < $V_{oc}$ < 700 mV). Finally, as the $I_0$ approaches 1 sun, the rate of $V_{oc}$ increase is reduced (Region


DOI: 10.1021/acs.jpclett.5b02014
J. Phys. Chem. Lett. 2015, 6, 4640–4645

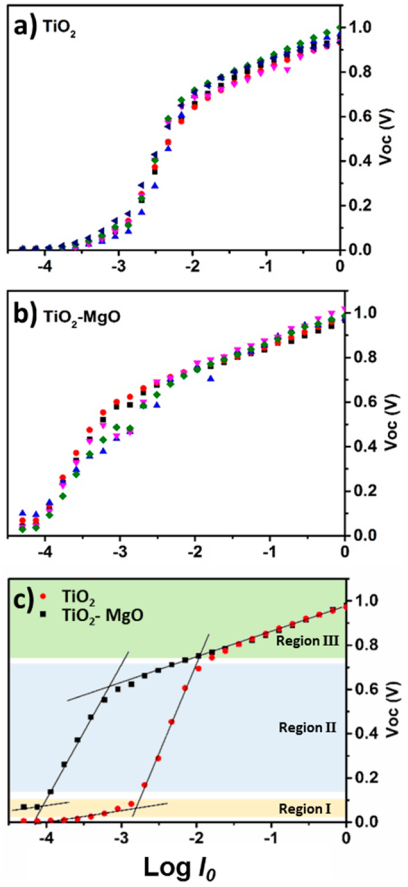


**Figure 3.** $V_{oc}$ vs log $I_0$ curves of several PSCs (different symbols) differing by the compact layer thickness: (a) $TiO_2$ PSC and (b) $TiO_2$−MgO PSC. The compact layer thicknesses ranged between 80−195 nm. (c) Comparison between a $TiO_2$ PSC and a $TiO_2$−MgO PSC with notation for all three regions.

III). All three regions are present in the $TiO_2$ and $TiO_2$−MgO samples; however, the rise in $V_{oc}$ in Region II in the $TiO_2$−MgO library begins at $I_0$ of $\sim 10^{-4}$ sun, compared with $\sim 10^{-3}$ sun for the $TiO_2$ sample. The use of the same hole transporting material (HTM) for both libraries limits the main difference of $V_{oc}$ to the electron quasi-Fermi level ($E_{Fn}$). This suggests an easier charge accumulation in the coated sample, with the following increase in $E_{Fn}$. However, at higher $I_0$ where both samples reach Region III, the values and behavior of the $V_{oc}$ are identical regardless of the MgO coating.

The statistical distribution of the $V_{oc}$ vs log $I_0$ slopes for the different regions is presented in Figure 4. In the first region, the

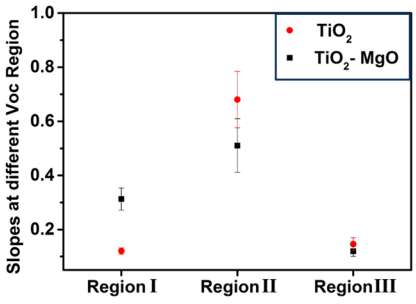


**Figure 4.** Average slopes (showing error bars) of the three different regions of the $V_{oc}$ vs log $I_0$ of the $TiO_2$ and $TiO_2$−MgO PSCs libraries.

increase of $V_{oc}$ with higher $I_0$ is slightly larger for the $TiO_2$−MgO samples, with the consequent higher slope. The situation is different in the intermediate region. The pronounced increase of $V_{oc}$, despite being shifted in $I_0$, shows similar high slopes for both samples. These large slopes (0.7 and 0.5 V per decade for $TiO_2$ and $TiO_2$−MgO respectively) suggest a recombination process independent of the voltage in this region. The charge carrier lifetimes at those voltages, estimated from the $V_{oc}$ decay analysis, confirm this (SI Figure S4). The decay measurements mimic the three regions at lower (<200 mV) medium (<700 mV) and higher $V_{oc}$s, and support an almost invariant recombination rate in the second region. This voltage-independent recombination could be explained with a preferred recombination path, such as energetic traps or defects,[28] but further analysis is needed to clarify this. The $V_{oc}$ vs log $I_0$ slopes of both samples coincide as the $I_0$ approaches 1 sun. These results imply a variation of the charge recombination mechanisms dominating the performance of the solar cell at different light intensities. It is important to remark that the $I_0$ required for the rise of $V_{oc}$ in Region II depends on the employed oxide, suggesting an $E_{Fn}$ determined by the recombination and density of states in the oxide.

Electrochemical measurements of the bare porous $TiO_2$ and $TiO_2$−MgO (both on compact $TiO_2$ layer) substrates offer a more detailed insight into the mechanisms controlling Region II, by explaining differences in the energetics. The cyclic voltammetry of the substrates (Figure 5a) revealed a subtle difference in the density of states of both samples. This difference, more visible when the accumulated charge is calculated (Figure 5b), is limited to the reduction of the density of states around 0 V vs Ag/AgCl with the MgO coating. This passivation is crucial to understand the illumination shift in Region II. With $TiO_2$ electrodes, the filling of the energetic states in the $TiO_2$ regulates $E_{Fn}$ at lower $I_0$. Once these states are being filled, $E_{Fn}$ and $V_{oc}$ can increase similarly in $TiO_2$ and $TiO_2$−MgO samples. The coincident slopes and $V_{oc}$ values at higher $I_0$ indicate that the same generation and recombination rates dominate the Region III in the analyzed samples. Therefore, the $E_{Fn}$ at the contact, and in accordance the achieved $V_{oc}$, must be determined here by the perovskite absorber. Thus, the perovskite contributes a further ~300 mV to the $V_{oc}$.

We propose that two working mechanisms, which are located in separated regimes, control the $V_{oc}$ of the PSC. At very low $I_0$, the $E_{Fn}$, in accordance with the $V_{oc}$, seems to be limited by the metal oxide. The intrinsic charge carrier density of the blocking layer[29] requires a higher photocarrier generation to significantly increase the $E_{Fn}$, as it happens in bulk heterojunction solar cells with the hole concentration.[30] Therefore, in this region, the increase of $V_{oc}$ is most likely determined by the hole Fermi level ($E_{Fp}$), with the accumulation of electrons taking place in the semiconductor oxide, similar to the case of dye sensitized solar cells (DSSC-like behavior).[15] At higher $I_0$, the $E_{Fn}$ in the perovskite directly determines the $V_{oc}$ regardless of the employed oxide (thin-film-like behavior). This hypothesis is supported by the low exciton binding energy in $CH_3NH_3PbX_3$,[31] which can result in a high electron and hole population within the perovskite under 1 sun illumination.[32]

Although the effects of the oxide are only visible at very low $I_0$, far from the AM1.5G conditions, the different voltage regimes can help to elucidate the working mechanisms of perovskite optoelectronics. At voltages 0 V < $V_{oc}$ < 700 mV, our devices seem to be affected by the employed metal oxide. In


DOI: 10.1021/acs.jpclett.5b02014
J. Phys. Chem. Lett. 2015, 6, 4640−4645

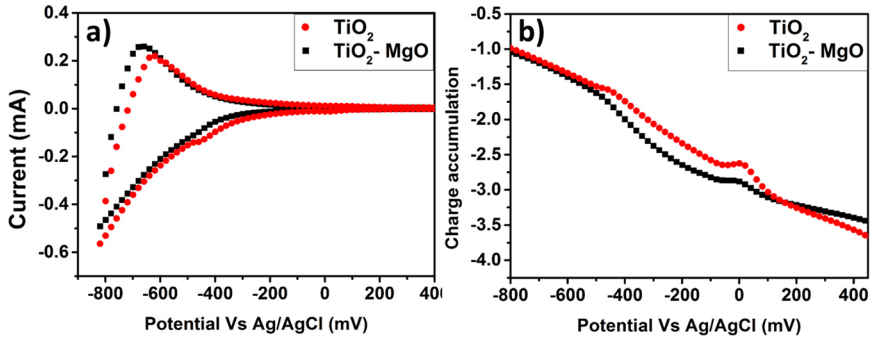


**Figure 5.** (a) Cyclic voltammetry measurements of mesoporous $TiO_2$ and $TiO_2$–MgO electrodes (both contained a $TiO_2$ compact layer). (b) Charge accumulation vs $V_{oc}$ calculated for both electrodes based on the cyclic voltammetry data.

this context, the operation of these solar cells at low voltages close to short-circuit conditions would be affected by the oxide semiconductor. The voltage sweep required to measure an *iV* curve would involve a change of regime between an oxide-determined $E_{Fn}$ and a perovskite-determined $E_{Fn}$ (from a DSSC to a thin-film-like behavior). The charge stored during this process could be one of the contributions to the hysteresis, a common topic in perovskite photovoltaics whose origin is still under debate.[33−37] Further studies of this aspect are currently ongoing. Although this study focuses on mesoporous $TiO_2$-based PSCs, we note that the dual behavior should also be expected in planar PSCs and noninjecting scaffolds based PSCs (i.e., mesoporous $Al_2O_3$), since both cases contain $TiO_2$ blocking layers as a selective contact. Therefore, we have fabricated mesoporous $Al_2O_3$ PSCs (with and without MgO coating) and performed similar $V_{oc}$ ($I_0$) measurements. The result of the $TiO_2$ and $Al_2O_3$ PSCs are practically identical (SI Figure S5a), and are in a good agreement with our explanation. This might be one of the reasons why inverted PSCs without $TiO_2$ are reported to have no or very small hysteresis.[38,39] The $Al_2O_3$–MgO samples also showed an earlier $V_{oc}$ rise at lower $I_0$ (SI Figure S5b). However, the effect was smaller than what we observed in the $TiO_2$–MgO samples. This led us to conclude that the compact $TiO_2$ blocking layer plays a significant and crucial role in determining the $V_{oc}$ at low light intensities (in the DSSC-like behavior region), with a much smaller contribution from the mesoporous $TiO_2$.

To summarize, we report on a statistical analysis of mesoporous PSCs, and evaluate the effect of the $TiO_2$ compact layer thickness and the MgO coating of the mesoscopic $TiO_2$. Our results depict an optimum $TiO_2$ blocking layer thickness (~135 nm) regardless of the coating. At this thickness, the power conversion efficiency is the largest and the dispersion of parameters is reduced. The analysis at low $I_0$ depicts three regions with different variation of the $V_{oc}$. We relate the first and second regions to the employed oxide, which is supported by $V_{oc}$ decay and cyclic voltammetry measurements. The $E_{Fn}$ and $V_{oc}$ at low $I_0$ are therefore determined by the oxide, similar to a DSSC case. In contrast, at $I_0$ close to 1 sun, the $V_{oc}$ of the solar cells seems to be solely determined by the perovskite absorber regardless of the employed oxide, such as in thin-films solar cells. By comparing the $V_{oc}$ ($I_0$) behavior in both $TiO_2$ and $Al_2O_3$ PSCs, we conclude that the compact $TiO_2$ blocking layer plays a significant and crucial role in determining the $V_{oc}$ (in the DSSC-like behavior region). Consequently, we would expect that a similar dual behavior would occur in planar PSCs that contain $TiO_2$ blocking layers as a selective contact. These results open a new interpretation of the working mechanisms of $CH_3NH_3PbX_3$ solar cells with $TiO_2$ n-type contacts.

## EXPERIMENTAL METHODS

The materials and chemicals used in this study for the device fabrication were purchased as follows: FTO glasses, TEC15 (Hartford Glass), titanium tetraisopropoxide (Sigma-Aldrich), $TiO_2$ paste (18NRT, Dyesol), $Al_2O_3$ (Degussa AG), $PbI_2$, $PbCl_2$ (Sigma-Aldrich), DMSO (Fisher Scientific), 2-propanol (J.T.Baker), spiro-OMeTAD (Merck), chlorobenzene (Alfa Aesar), acetonitrile (J.T.Baker), bis(trifluoromethylsulfonyl)-imide lithium salt (Sigma-Aldrich), and 4-*tert*-butylpyridine, (Sigma-Aldrich). The $Al_2O_3$ paste was prepared using a procedure described elsewhere.[40] TEC 15 fluorine-doped tin oxide coated glass (dimensions: 71 × 71 $mm^2$) was used as the substrate for the device fabrication. Each substrate was thoroughly cleaned with detergent, water, and ethanol before treatment with argon plasma for 4 min. The compact gradient $TiO_2$ blocking layer was deposited by a spray pyrolysis system in a procedure described elsewhere.[25] A precursor solution of 0.1 M titanium-tetraisopropoxide and acetyl acetone (1:1 ratio) in ethanol was sprayed on the preheated (450 °C) substrates and the thickness of the blocking layer was calculated by using optical modeling. The mesoporous $TiO_2$ and $Al_2O_3$ scaffolds were 250−300 nm thick, deposited from diluted pastes (diluted with ethanol at 1:10 ratio) on the $TiO_2$ blocking layer by spin coating at 5000 rpm for 30 s. The substrates were then annealed at 550 °C for 90 min. The deposition of the MgO coating is described elsewhere.[41]

A mixed lead halide solution was prepared using a 1M:0.06 M ratio of $PbI_2$:$PbCl_2$ dissolved in DMSO and then stirred at 80 °C overnight. The MAI solution (32 mg/mL in 2-propanol) was heated to 60 °C before use. The deposition of perovskite was performed by spin coating $PbI_{2-x}Cl_x$ at 4000 rpm for 60 s on mesoporous $TiO_2$ electrode and the film was subsequently annealed at 100 °C for 60 min. Afterward, the films were dipped in the MAI solution for 2 min followed by washing with 2-propanol. A 50 μL aliquot of toluene was spun at 4000 rpm onto the perovskite film, which was exposed to MAI vapors for 60 min. The exposure was performed by holding the substrate upside down in a Pyrex glass box containing 200 mg of MAI (methylammonium iodide) powder heated at 140 °C. After the vapor treatment, the substrates were annealed on a hot plate at 100 °C for 90 min. The synthesis of the MAI powder is described elsewhere.[42]

The hole transport material (HTM), spiro-OMeTAD, was dissolved in chlorobenzene (72 mg/mL) with the addition of 34 μL (540 mg/mL in acetonitrile) of bis-



DOI: 10.1021/acs.jpclett.5b02014
J. Phys. Chem. Lett. 2015, 6, 4640−4645

(trifluoromethylsulfonyl)imide lithium salt (LiTFSI), and 58 μL (80 mM) of 4-*tert*-butylpyridine (TBP). The HTM solution was spin coated onto the perovskite films at 4000 rpm for 30 s. The substrates were kept in a drybox (air environment) overnight under dark conditions to dope the HTM with oxygen. A grid of 13 × 13 back contact silver electrodes (100 nm thick) was thermally evaporated on each substrate using a mechanical mask, forming a total of 169 devices (with cell area of ∼0.026 cm2) fabricated on one substrate. Finally, *iV* measurements were performed using a home-built automated scanning *iV* system described elsewhere[25] (note: each PSC in the library was illuminated individually without light soaking). For statistical analysis, we used the data taken from 121 devices (in each library) to eliminate any misinterpretation of data from PSCs in the edges of the library.

The $V_{oc}$ vs log $I_0$ plots were acquired by measuring the stabilized $V_{oc}$ (i.e., held at open-circuit conditions without a voltage scan) in 25 different light intensities ranging from 0.00005−1 Sun. The $V_{oc}$ decay plots were acquired by illuminating the PSC with different light intensities in a system that is reported elsewhere. After the $V_{oc}$ stabilized the light was turned off and the $V_{oc}$ decay was recorded in the dark. The cyclic voltammetry measurements are performed on compact layer/mesoporous MgO samples, with and without MgO coating. The buffer $LiClO_4$ solution (pH 2) and was purged with nitrogen gas before measurements for 30 min. Reference and counter electrodes were Ag/AgCl and Pt coated FTO glass and the scan rate was 100 mV/s.

## ■ ASSOCIATED CONTENT

### Supporting Information

The Supporting Information is available free of charge on the ACS Publications website at DOI: 10.1021/acs.jpclett.5b02014.

*iV* scans of the highest efficiency PSCs, $J_{sc}$, fill factor of parameters (from both libraries) and the dark current vs $TiO_2$ compact layer thickness, $V_{oc}$ decay of PSCs, and more $V_{oc}$ ($I_0$) of $Al_2O_3$ PSCs are presented. (PDF)

## ■ AUTHOR INFORMATION


### Corresponding Authors

*A. Zaban. E-mail: zabana@mail.biu.ac.il.

*P. P. Boix. E-mail: pbpablo@ntu.edu.sg.


### Author Contributions

L.G. and R.G. have contributed equally to this work.

### Notes

The authors declare no competing financial interest.

## ■ ACKNOWLEDGMENTS

We wish to thank Dr. Larissa Grinis for her valuable assistance. We thank the Israel Strategic Alternative Energy Foundation (I-SAEF) and the "Tashtiyot" Program of the Israeli Ministry of Science & Technology for funding this research. Fellowship for L.G. is from the European Union Seventh Framework Program Destiny Project, under grant 316494 is acknowledged. P.P.B. would like to acknowledge the funding from Singapore NRF through the Competitive Research Program: NRF-CRP4-2008-03 and NRF-CRP14-2014-03.

## ■ REFERENCES


(1) Lee, M. M.; Teuscher, J.; Miyasaka, T.; Murakami, T. N.; Snaith, H. J. Efficient Hybrid Solar Cells Based on Meso-Superstructured Organometal Halide Perovskites. *Science* **2012**, *338*, 643−647.

(2) Kim, H.-S.; Lee, C.-R.; Im, J.-H.; Lee, K.-B.; Moehl, T.; Marchioro, A.; Moon, S.-J.; Humphry-Baker, R.; Yum, J.-H.; Moser, J. E.; et al. Lead Iodide Perovskite Sensitized All-Solid-State Submicron Thin Film Mesoscopic Solar Cell with Efficiency Exceeding 9%. *Sci. Rep.* **2012**, *2*, 591.

(3) Yang, W. S.; Jun, H. N.; Jeon, N. J.; Kim, Y. C.; Ryu, S.; Seo, J.; Seok, S. Il. High-Performance Photovoltaic Perovskite Layers Fabricated through Intramolecular Exchange. *Science* **2015**, *348*, 1234−1237.

(4) Dong, Q.; Fang, Y.; Shao, Y.; Mulligan, P.; Qiu, J.; Cao, L.; Huang, J. Electron-Hole Diffusion Lengths > 175 μm in Solution-Grown $CH_3NH_3PbI_3$ Single Crystals. *Science* **2015**, *347*, 967−970.

(5) Stranks, S. D.; Eperon, G. E.; Grancini, G.; Menelaou, C.; Alcocer, M. J. P.; Leijtens, T.; Herz, L. M.; Petrozza, A.; Snaith, H. J. Electron-Hole Diffusion Lengths Exceeding 1 Micrometer in an Organometal Trihalide Perovskite Absorber. *Science* **2013**, *342*, 341−344.

(6) De Wolf, S.; Holovsky, J.; Moon, S.-J.; Loper, P.; Niesen, B.; Ledinsky, M.; Haug, F.; Yum, J.; Ballif, C. Organometallic Halide Perovskites: Sharp Optical Absorption Edge and Its Relation to Photovoltaic Performance. *J. Phys. Chem. Lett.* **2014**, *5*, 1035−1039.

(7) Kulkarni, S. A.; Baikie, T.; Boix, P. P.; Yantara, N.; Mathews, N.; Mhaisalkar, S. Band-Gap Tuning of Lead Halide Perovskites Using a Sequential Deposition Process. *J. Mater. Chem. A* **2014**, *2*, 9221−9225.

(8) Xing, G.; Mathews, N.; Lim, S. S.; Yantara, N.; Liu, X.; Sabba, D.; Gratzel, M.; Mhaisalkar, S.; Sum, T. C. Low-Temperature Solution-Processed Wavelength-Tunable Perovskites for Lasing. *Nat. Mater.* **2014**, *13*, 476−480.

(9) Moehl, T.; Im, J. H.; Lee, Y. H.; Domanski, K.; Giordano, F.; Zakeeruddin, S. M.; Dar, M. I.; Heiniger, L.-P.; Nazeeruddin, M. K.; Park, N.; et al. Strong Photocurrent Amplification in Perovskite Solar Cells with a Porous $TiO_2$ Blocking Layer under Reverse Bias. *J. Phys. Chem. Lett.* **2014**, *5*, 3931−3936.

(10) Gil-Escrig, L.; Longo, G.; Pertegás, A.; Roldán-Carmona, C.; Soriano, a; Sessolo, M.; Bolink, H. J. Efficient Photovoltaic and Electroluminescent Perovskite Devices. *Chem. Commun.* **2015**, *51*, 569−571.

(11) Tan, Z.-K.; Moghaddam, R. S.; Lai, M. L.; Docampo, P.; Higler, R.; Deschler, F.; Price, M.; Sadhanala, A.; Pazos, L. M.; Credgington, D.; et al. Bright Light-Emitting Diodes Based on Organometal Halide Perovskite. *Nat. Nanotechnol.* **2014**, *9*, 687−692.

(12) Xiao, Z.; Yuan, Y.; Shao, Y.; Wang, Q.; Dong, Q.; Bi, C.; Sharma, P.; Alexei, G.; Jinsong, H. Giant Switchable Photovoltaic Effect in Organometal Trihalide Perovskite Devices. *Nat. Mater.* **2015**, *14*, 193−198.

(13) Bertoluzzi, L.; Sanchez, R. S.; Liu, L.; Lee, J.-W.; Mas-Marza, E.; Han, H.; Park, N.-G.; Mora-Sero, I.; Bisquert, J. Cooperative Kinetics of Depolarization in $CH_3NH_3PbI_3$ Perovskite Solar Cells. *Energy Environ. Sci.* **2015**, *8*, 910−915.

(14) Boix, P. P.; Nonomura, K.; Mathews, N.; Mhaisalkar, S. G. Current Progress and Future Perspectives for Organic/inorganic Perovskite Solar Cells. *Mater. Today* **2014**, *17*, 16−23.

(15) O'Regan, C. B.; Gratzel, M. A Low-Cost, High-Efficiency Solar Cell Based on Dye-Sensitized Colloidal $TiO_2$ Films. *Nature* **1991**, *353*, 737−740.

(16) Bach, U.; Lupo, D.; Comte, P.; Moser, J. E.; Weissortel, F.; Salbeck, J.; Spreitzer, H.; Gratzel, M. Solid-State Dye-Sensitized Mesoporous $TiO_2$ Solar Cells with High Photon-to-Electron Conversion Efficiencie. *Nature* **1998**, *395*, 583−585.

(17) Ryu, S.; Noh, N. H.; Jeon, N. J.; Kim, Y. C.; Yang, W. S.; Seo, J.; Seok, S. Il. Voltage Output of Efficient Perovskite Solar Cells with High Open-Circuit Voltage and Fill Factor. *Energy Environ. Sci.* **2014**, *7*, 2614−2618.

(18) Juarez-perez, E. J.; Wußler, M.; Fabregat-Santiago, F.; Lakus-Wollny, K.; Mankel, E.; Mayer, T.; Jaegermann, W.; Mora-sero, I. Role of the Selective Contacts in the Performance of Lead Halide Perovskite Solar Cells. *J. Phys. Chem. Lett.* **2014**, *5*, 680−685.

(19) Suarez, B.; Gonzalez-Pedro, V.; Ripolles, T. S.; Sanchez, R. S.; Otero, L.; Mora-Sero, I. Recombination Study of Combined Halides




DOI: 10.1021/acs.jpclett.5b02014
*J. Phys. Chem. Lett.* 2015, 6, 4640−4645

(Cl, Br, I) Perovskite Solar Cells. *J. Phys. Chem. Lett.* **2014**, *5*, 1628−1635.
(20) Shen, Q.; Ogomi, Y.; Chang, J.; Tsukamoto, S.; Kukihara, K.; Oshima, T.; Osada, N.; Yoshino, K.; Katayama, K.; Toyoda, T.; et al. Charge Transfer and Recombination at the Metal oxide/$CH_3NH_3PbClI_2$/spiro-OMeTAD Interfaces: Uncovering the Detailed Mechanism behind High Efficiency Solar Cells. *Phys. Chem. Chem. Phys.* **2014**, *16*, 19984−19992.
(21) Listorti, A.; Juarez-Perez, E. J.; Frontera, C.; Roiati, V.; Garcia-Andrade, L.; Colella, S.; Rizzo, A.; Ortiz, P.; Mora-Sero, I. Effect of Mesostructured Layer upon Crystalline Properties and Device Performance on Perovskite Solar Cells. *J. Phys. Chem. Lett.* **2015**, *6*, 1628−1637.
(22) Edri, E.; Kirmayer, S.; Henning, A.; Mukhopadhyay, S.; Gartsman, K.; Rosenwaks, Y.; Hodes, G.; Cahen, D. Why Lead Methylammonium Tri-Iodide Perovskite-Based Solar Cells Require a Mesoporous Electron Transporting Scaffold (but Not Necessarily a Hole Conductor). *Nano Lett.* **2014**, *14*, 1000−1004.
(23) Salvador, P.; Hidalgo, M. G.; Zaban, A.; Bisquert, J. Illumination Intensity Dependence of the Photovoltage in Nanostructured $TiO_2$ Dye-Sensitized Solar Cells. *J. Phys. Chem. B* **2005**, *109*, 15915−15926.
(24) Zaban, A.; Greenshtein, M.; Bisquert, J. Determination of the Electron Lifetime in Nanocrystalline Dye Solar Cells by Open-Circuit Voltage Decay Measurements. *ChemPhysChem* **2003**, *4*, 859−864.
(25) Anderson, A. Y.; Bouhadana, Y.; Barad, H. N.; Kupfer, B.; Rosh-Hodesh, E.; Aviv, H.; Tischler, Y. R.; Rühle, S.; Zaban, A. Quantum Efficiency and Bandgap Analysis for Combinatorial Photovoltaics: Sorting Activity of Cu-O Compounds in All-Oxide Device Libraries. *ACS Comb. Sci.* **2014**, *16*, 53−65.
(26) Rühle, S.; Barad, H. N.; Bouhadana, Y.; Keller, D. A.; Ginsburg, A.; Shimanovich, K.; Majhi, K.; Lovrincic, R.; Anderson, A. Y.; Zaban, A. Combinatorial Solar Cell Libraries for the Investigation of Different Metal Back Contacts for $TiO_2$-$Cu_2O$ Hetero-Junction Solar Cells. *Phys. Chem. Chem. Phys.* **2014**, *16*, 7066−7073.
(27) Rühle, S.; Anderson, A. Y.; Barad, H. N.; Kupfer, B.; Bouhadana, Y.; Rosh-Hodesh, E.; Zaban, A. All-Oxide Photovoltaics. *J. Phys. Chem. Lett.* **2012**, *3*, 3755−3764.
(28) Gottesman, R.; Tirosh, S.; Barad, H.-N.; Zaban, A. Direct Imaging of the Recombination/Reduction Sites in Porous $TiO_2$ Electrodes. *J. Phys. Chem. Lett.* **2013**, *4*, 2822−2828.
(29) Kavan, L.; Tétreault, N.; Moehl, T.; Grätzel, M. Electrochemical Characterization of $TiO_2$ Blocking Layers for Dye-Sensitized Solar Cells. *J. Phys. Chem. C* **2014**, *118*, 16408−16418.
(30) Boix, P. P.; Wienk, M. M.; Janssen, R. A. J.; Garcia-Belmonte, G. Open-Circuit Voltage Limitation in Low-Bandgap Diketopyrrolopyrrole-Based Polymer Solar Cells Processed from Different Solvents. *J. Phys. Chem. C* **2011**, *115*, 15075−15080.
(31) D'Innocenzo, V.; Grancini, G.; Alcocer, M. J. P.; Kandada, A. R. S.; Stranks, S. D.; Lee, M. M.; Lanzani, G.; Snaith, H. J.; Petrozza, A. Excitons versus Free Charges in Organo-Lead Tri-Halide Perovskites. *Nat. Commun.* **2014**, *5*, 3586.
(32) Manser, J. S.; Kamat, P. V. Band Filling with Free Charge Carriers in Organometal Halide Perovskites. *Nat. Photonics* **2014**, *8*, 737−743.
(33) Tress, W.; Marinova, N.; Moehl, T.; Zakeeruddin, S. M.; Nazeeruddin, M. K.; Gratzel, M. Understanding the Rate-Dependent J−V Hysteresis, Slow Time Component, and Aging in $CH_3NH_3PbI_3$ Perovskite Solar Cells: The Role of a Compensated Electric Field. *Energy Environ. Sci.* **2015**, *8*, 995−1004.
(34) Yang, T.-Y.; Gregori, G.; Pellet, N.; Gratzel, M.; Maier, J. The Significance of Ion Conduction in a Hybrid Organic-Inorganic Lead-Iodide-Based Perovskite Photosensitizer. *Angew. Chem., Int. Ed.* **2015**, *54*, 7905.
(35) Kim, H.-S.; Kim, S. K.; Kim, B. J.; Shin, K.-S.; Gupta, M. K.; Jung, H. S.; Kim, S.-W.; Park, N.-G. Ferroelectric Polarization in $CH_3NH_3PbI_3$ Perovskite. *J. Phys. Chem. Lett.* **2015**, *6*, 1729−1735.
(36) Gottesman, R.; Gouda, L.; Kalanoor, B. S.; Haltzi, E.; Tirosh, S.; Rosh-Hodesh, E.; Tischler, Y.; Quarti, C.; Mosconi, E.; Angelis, F. De; et al. Photoinduced Reversible Structural Transformations in Free-Standing $CH_3NH_3PbI_3$ Perovskite Films. *J. Phys. Chem. Lett.* **2015**, *6*, 2332−2338.
(37) Azpiroz, J. M.; Mosconi, E.; Bisquert, J.; De Angelis, F. Defect Migration in Methylammonium Lead Iodide and Its Role in Perovskite Solar Cell Operation. *Energy Environ. Sci.* **2015**, *8*, 2118−2127.
(38) Heo, J. H.; Han, H. J.; Kim, D.; Ahn, T. K.; Im, S. H. Hysteresis-Less Inverted $CH_3NH_3PbI_3$ Planar Perovskite Hybrid Solar Cells with 18.1% Power Conversion Efficiency. *Energy Environ. Sci.* **2015**, *8*, 1602−1608.
(39) Shao, Y.; Xiao, Z.; Bi, C.; Yuan, Y.; Huang, J. Origin and Elimination of Photocurrent Hysteresis by Fullerene Passivation in $CH_3NH_3PbI_3$ Planar Heterojunction Solar Cells. *Nat. Commun.* **2014**, *5*, 5784.
(40) Hod, I.; Tachan, Z.; Shalom, M.; Zaban, A. Characterization and Control of the Electronic Properties of a NiO Based Dye Sensitized Photocathode. *Phys. Chem. Chem. Phys.* **2013**, *15*, 6339−6343.
(41) Tachan, Z.; Hod, I.; Shalom, M.; Grinis, L.; Zaban, A. The Importance of the $TiO_2$/quantum Dots Interface in the Recombination Processes of Quantum Dot Sensitized Solar Cells. *Phys. Chem. Chem. Phys.* **2013**, *15*, 3841−3845.
(42) Gottesman, R.; Haltzi, E.; Gouda, L.; Tirosh, S.; Bouhadana, Y.; Mosconi, E.; De Angelis, F.; Zaban, A. Extremely Slow Photoconductivity Response of $CH_3NH_3PbI_3$ Perovskites Suggesting Structural Changes under Working Conditions. *J. Phys. Chem. Lett.* **2014**, *5*, 2662−2669.


DOI: 10.1021/acs.jpclett.5b02014
*J. Phys. Chem. Lett.* 2015, 6, 4640−4645